Regular Article

Hydrogen embrittlement effect observed by in-situ hydrogen plasma charging on a ferritic alloy

Di Wan*

di.wan@ntnu.no

Yun Deng

Afrooz Barnoush

Department of Mechanical and Industrial Engineering, Norwegian University of Science and Technology, Richard Birkelands vei 2B, 7491 Trondheim, Norway

*Corresponding author.

Abstract

To study the hydrogen embrittlement (HE) effect, a novel in-situ slow strain rate tensile test together with in-situ hydrogen (H) charging by H-plasma was conducted in an environmental scanning electron microscope (ESEM). The introduction of H-plasma gave a reduction in tensile elongation by about 5% in comparison with a reference test in vacuum. Fractographic observation clearly showed the difference in the resulted features on the fracture surfaces. Electron backscatter diffraction (EBSD) was conducted to elucidate the characteristics of the cracks. Such investigations can help to refresh the existing knowledge in HE study.

Keywords: hHydrogen embrittlement; iIn-situ test; Fe-3wt-%Si; pPlasma; eCrack

Hydrogen embrittlement (HE) is a well-acknowledged phenomenon in metals. It draws much scientists' and engineers' attention because it can lead to catastrophic failure of an industrial structure. Researchers use different methods to charge a test piece with hydrogen (H) and study the behavior of the material during or after charging. A common method is to use H_2 gas as the environment, for example Vehoff [1,2] used gaseous H to study the H effect on the fracture behavior of ferritic steels. More examples can be found in Ref. [3–12]. Furthermore, electrochemical cathodic charging is also commonly used, for example Wang et al. [13] used cathodic charging with an in-situ tensile test to study the effect of H on mobile dislocations, and the H concentrations were also determined. Other examples can be found in Ref. [14–22] as well. There is also a smart method for special materials, for example, Deng et al. [23,24] and Rogne et al. [25] used water vapor to charge Fe-Al intermetallic alloys since the H_2O molecule can react with Al, producing alumina and H to invade the matrix.

Due to the high diffusivity of H in body-centered cubic (BCC) lattice [13], it is always critical to have H pre-charging on the test piece because H can diffuse out even during a short transferring procedure. Therefore, in-situ H-charging is favored for the HE study of BCC structures.

Currently, in-situ charging of ferritic steel is either done in high pressure hydrogen gas or under electrochemical control by cathodic H-charging. This makes the high-resolution observation of the sample during deformation challenging.

Environmental scanning electron microscopy (ESEM) combined with miniaturized tensile stages provides a unique possibility to test the effect of H on mechanical deformation, however the limited maximum pressure inside the chamber and restrictions on the possible gases at that pressure in the chamber from the manufacturer hinders the HE tests inside the ESEM. At low pressures, the fugacity of H is not enough to have adequate physisorption and dissociation of the H_2 molecules on the surface to observe HE within a reasonable time scale. Converting H_2 gas to H plasma before letting it enter the ESEM chamber will increase the H fugacity in the chamber and provide possibilities to observe the HE processes inside the ESEM.

Narita [26] used H glow charging to study the embrittlement effect in a Fe-Si system with a tensile test on single crystals and concluded that this method is capable of charging the samples with enough H to reveal an embrittlement effect without severe surface damage. Kimura and Birnbaum [27] observed that that H-plasma charging can cause a softening effect in the flow stress of pure iron samples. A recent work from Malitckii et al. [28] used H-rich plasma at elevated temperatures to charge two kinds of steels and successfully revealed the HE effect on them.

In this paper, we show that the introduction of low pressure H-plasma in ESEM chamber can provide a possibility to study the HE of a ferritic alloy with in-situ mechanical testing. The limitation in in-situ investigation has been discussed. Moreover, ex-situ characterization was carried out to study the details of the tested specimen. Such investigations can help us refresh the knowledge in HE.

Simple ferritic Fe-3wt.%Si alloy with the composition shown in Table 1 was used in this study. The as-received material has a coarse grain size of 300 μm. This simple microstructure makes the alloy a perfect model material to establish the methodology (e.g. [1,2,29–33]).Tensile specimens were cut from the raw material by electrical discharge machining (EDM) to a dog-bone shape with the gauge geometry of 20 mm × 6 mm × 2 mm. Grinding to #4000 emery paper followed by 3 μm and 1 μm diamond paste polishing plus final electropolishing was adopted to make sure the tested surfaces were flat and smooth without residual deformation. The tensile/compression module from Kammrath & Weiss GmbH (Germany) was used for mechanical testing inside a Quanta 650 ESEM (Thermo Fisher Scientific Inc., USA). The engineering strain rate was chosen to be 10^{-5} s^{-1} in order to provide enough time for H adsorption and diffusion. After fracture, the half-specimens were taken out for further characterization. For H-charging, an Evactron Model 25 Zephyr Plasma Cleaner (XEI Scientific, USA) was used with gaseous H_2 as a process gas from a hydrogen generator. It should be noted that remote plasma was applied in this cleaner. With this method, the interaction between plasma and material occurs at a location that is remote from the plasma afterglow. In other words, only active plasma would participate in the interactions with the material, such that the specimen surface can prevent from heating, contaminating and damaging effects.

Table 1 Chemical composition of the investigated material.

alt-text: Table 1

Elem.	C	Si	Mn	P	S	Cr	Ni	Mo
wt.%	0.018	3.000	0.055	0.008	0.003	0.010	0.006	0.003

Elem.	Cu	Al	Ti	Nb	V	B	Zr	Fe
wt.%	0.013	0.015	0.001	0.002	0.001	0.0002	0.0010	Bal.

Fig. 1 shows the experimental setup of the SEM chamber. The plasma cleaner was connected to the SEM chamber via a flange, and the hydrogen generator was connected to the working gas inlet of the plasma cleaner. The tensile specimen was installed into the tensile/compression module connecting to an external controlling unit via another flange. With this setup, in-situ mechanical testing with in-situ H-charging can be realized. In-situ observation by normal SEM mode is limited and we are discussing the possibilities for imaging at low pressure H-plasma with the ESEM manufacturer. To the authors' knowledge, no reports on imaging by high voltage electrons with H-plasma presenting have been found. According to the communications with the company, in-situ imaging with high-voltage in H environment is potentially unsafe. Since H is extremely flammable, there is a likelihood of arcing in the chamber from the detectors and this is extremely likely to cause the H to ignite. For this reason, the investigations in this study could only be done when the chamber is completely evacuated to high-vacuum state.

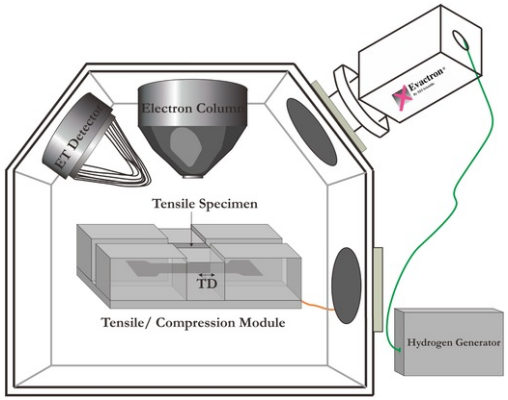

Fig. 1 Experimental setup of the SEM chamber (TD: tensile direction).

alt-text: Fig. 1

The stress-strain curves for the tensile tests are shown in Fig. 2. It should be noted that the stress is calculated by dividing the load over the cross-section area in the gauge range, which was re-measured after preparation since grinding and polishing could change the geometry of the specimen. The tests were denoted as Vac case (tested in vacuum) and H case (tested in H-plasma), respectively. The H test was done by stopping the test at the ultimate tensile strength (UTS) range from the Vac test for one hour to give more time for H uptake into the lattice under enhanced solubility effect of the tensile stress as well as exposure of the oxide free surface. From the curves, the two specimens had similar behaviors in the elastic range and behaved similarly up to the UTS range with a slight hardening effect in the H case. But the H-charged specimen had a reduction in the elongation to fracture by about 5% and the crack propagation procedure was much faster and more unstable. It is difficult to define the crack initiation from the stress-strain curves, but it can be seen qualitatively that the crack was growing in a more stable manner in Vac than in H case, which showed a sudden failure. A supplementary video was attached to this work, showing the relatively stable crack propagation procedure of the Vac case. This procedure corresponds to the part highlighted by blue dash-lines in Fig. 2. For the H case, due to technical limitations, no imaging is possible during the plasma charging and pictures can only be taken after interrupting the plasma and evacuating the chamber from H. We are currently discussing with the ESEM manufacturer for modification to try to make this imaging process possible.

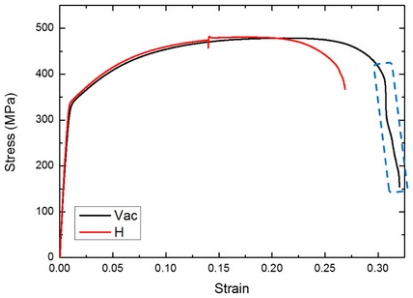

Fig. 2 Stress-strain curves of the investigated specimens (the highlighted part corresponds to the crack propagation procedure, which is shown by a video in supplementary files).

alt-text: Fig. 2

Fig. 3 shows the fracture surfaces of the specimens after final fracture in Vac and in H case, respectively. The reduction in area from calculation is 61.4% for Vac and 50.1% for H case, respectively. The fracture surfaces showed generally transgranular type, regardless of H-plasma charging. The ductile feature (dimples) is highlighted by yellow dash-lines. A large area fraction (about 75% of the whole fracture surface) of dimples can be found in the Vac case, which indicates the crack growth procedure was in a more ductile manner when H was absent. While in the H case, most of the area shows brittle transgranular cleavage-like features with only a limited area fraction (about 10% of the whole fracture surface) of ductile features. Besides, many secondary cracks are observed on the fracture surface in the H case while these are not seen in the Vac case. Fig. 3b and c show the magnified dimple features in Vac case, with b showing inclusion spots in dimples and c showing pure dimple structure. This indicates a ductile behavior of this specimen in Vac, regardless of the presence of small inclusions. Fig. 3e and f reveal detailed fracture surface of the H case showing cleavage-like features. Fig. 3e shows typical brittle facets on the fracture surface with microligaments and river-lines. Fig. 3f shows clear river-lines with secondary cracks on the fracture surface. This observation is consistent with previous works on the similar alloy system [2,32,34]. The river-patterns are formed from cleavage and are characteristic for brittle fracture mechanism. The appearance of these features indicates a brittle, though plasticity-related cracking process. Mine et al. [35] did a micro-tensile test with H on austenitic steels, and found similar quasi-cleavage fracture features. They concluded that a high H concentration can lead to localized shear and form quasi-cleavage fracture.

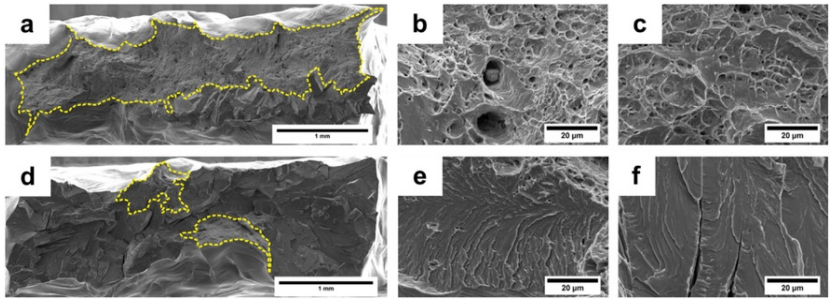

Fig. 3 Fracture surfaces of the fractured tensile specimens (a-c: in vacuum; d-f: with H-plasma charging; b, c and e, f are magnified representative features in a and d, respectively; highlighted areas enclosed by yellow dash-lines are ductile part with an are fraction of 75% for Vac, and 10% for H, respectively; detailed discussion in text). (For interpretation of the references to colour in this figure legend, the reader is referred to the web version of this article.)

alt-text: Fig. 3

Fig. 4 gives the top-view on the specimens after tensile fracture. The magnified zone in the lower right corner of Fig. 4b is from the highlighted area in the middle and the {100} traces are from electron backscatter diffraction (EBSD) analysis on the corresponding cracking grains. The Vac case shows a shear fracture along the direction approximately 45° to the tensile direction. This is not rare for materials that experience ductile fracture failure since 45° is the direction of the principal shear stress during monotonic tensile loading. The H case shows the main crack nearly perpendicular to the tensile direction. The final widths of the specimens were measured with showing no significant difference between the two cases. It is interesting that many secondary cracks (eight as measured in the magnified zone in Fig. 4b) can also be found in this view in the H case, while the Vac case does not show similar features. Thus, the appearance of these secondary cracks can be ascribed to the H effect. The secondary cracks form clearly a relationship of 90° between each other. A further EBSD test was done on the fractured specimen and confirmed the direction being [100]. This is rational because {100} plane system is the cleavage plane system of BCC lattice, and this implies a possible H-induced cleavage transition mechanism.

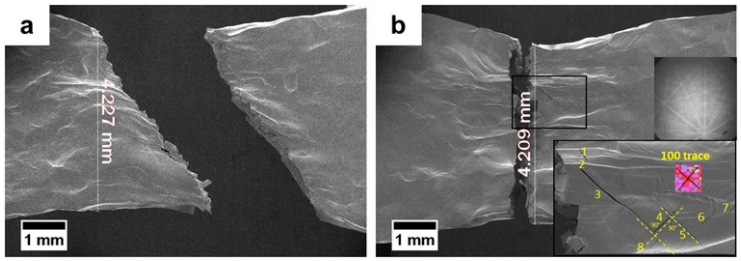

Fig. 4 Top-view on the tensile specimens after final fracture (a: in vacuum; b: in H-plasma; the structure shown in the lower right corner of b is highlighted by the black square, and the {100} traces were measured by EBSD with a representative Kikuchi pattern from the raw data).

alt-text: Fig. 4

It is generally acknowledged that there are two important necessary conditions to cause HE effect, namely high enough stress and adequate H concentration. In the present study, we used a relatively low strength steel. According to the standard, steels with yield strength below 400 MPa are immune against HE. Therefore, the tensile behavior of the H case was the same as the Vac case before the UTS was reached, and deviation of the stress-strain curve happened after the stress level in the steel reached to higher values and close to the UTS (see Fig. 2). When necking happened, the localized deformation led to a localized stress field that can enhance local H uptake and cause embrittlement effect at the necked area. It is assumed that the combination of local high stress condition and high H concentration caused the HE effect. This can be the reason that the stress-strain curve of the H case started to deviate after necking, as seen in Fig. 2. In this case, the HE actually took place in a material that has been hardened up to the UTS level, and the real HE effect should be considered from the critical status. If we define the HE effect in percentage could be calculated by the elongation loss over the full elongation range in the Vac case, the value from the original curves should be about 18%; while if we assume the HE starts from the hardened status, this value changes to about 33%.

An important parameter in HE study is the H content. We used a fixed H_2 flow rate of about 250 ml/min from the hydrogen generator. The chamber pressure for plasma excitation is around 40 Pa in this study,

and when the plasma is excited, the working pressure can reach an approximately fixed value of 70–80 Pa, with an increment of about 30–40 Pa. Vesel et. al et al. [36] in comparable H-plasma formation condition used fiber-optic catalytic probe and measured a density of H atom in the range of 2.5×10^{21} atom/m^3 [36] which shows that the atomic H is the main expected constituent of the plasma in the vicinity of the source. The fugacity of the dissociated H atoms will be far above 80 Pa as reported by Bond et. al et al. and can reach values as high as several MPa [37]. According to the conclusions in Ref. [38] that HE doesn't occur with insufficient H concentration, the amount of H in this work revealed to be enough to cause HE.

The H-plasma charging procedure gives a minor influence on the strength of the material, which is consistent with the work from Malitckii [28] and Depover [16,19] on different kinds of steels with other charging methods. Birnbaum [39] reported that H in solid solution increased the mobilities of dislocations and could give a macroscopic softening in the presence of slip localization. In this study, however, no significant proof of slip localization was found yet and neither softening effect when H was present. One possible reason is that the dislocations were motivated by H to contribute to cracks formation rather than forming local slip lines. The results in Fig. 3d–f all show that the cracks were formed inside the matrix of the specimen in a transgranular and brittle manner.

Kimura et al. [38] reported an important effect of H in iron is that H reduces the {100} cleavage stress, which is one of the fundamental mechanisms of HE in iron. From the classical theory of dislocation interactions in BCC lattice [40], a [-1-11] type dislocation and a [111] type dislocation in BCC lattice can meet and produce an immobile [001] type dislocation, and the accumulation of this type of immobile dislocations can lead to a cleavage fracture of (001) planes. This is believed to be a plasticity-related cleavage fracture mechanism. Chen et al. [34] concluded that the cracking induced by external H in Fe-3wt-%Si single crystal is cleavage process accompanied with severe plasticity.

One hypothesis proposed by the work from Ref. [24, 25, 41] is that during deformation, the stress was localized at the necking area when the specimen started to deform unstably. The stress localization activated multi slip systems in the necking region. There, the H-dislocation interaction was strongly intensified and the dislocation motion was further blocked by increasing H pinning effect [24,42]. A common finding of these works is that when H is absent, the crack tip keeps blunting, while when H is presenting, the principal crack keeps sharp and leads to brittle cleavage fracture. The resulting fracture surfaces are similar to the present study: voids and dimples were found in Vac case and flat, cleavage-like fracture were found in H case. Similar phenomena were found in FeAl [23,24], Fe3Al [25] and Fe-3wt-%Si [41] by micro-cantilever bending test with in-situ H-charging, and explained schematically and systematically in Ref. [24].

To sum up, the present study used a novel in-situ setup for HE research combining H-charging, mechanical testing and investigation. It is clearly shown that this study reveals the HE effect of a ferritic Fe-3wt%Si alloy during slow strain rate monotonic tension under H-plasma charging. The elongation to fracture got a reduction by about 5% as well as the failure procedure shifted to a faster and more brittle manner. The flow stress of the material got a minor influence from H-plasma. The microstructure observation reveals that the H-free specimen has more ductile features than the H-charged one. An ideal outcome would be that the HE effect can be observed during mechanical testing by switching on and off the H-source with showing a shift in the mechanical behavior or microstructure in a well-defined specimen, by which manner the original mechanism of H on the test piece can be directly observed and depicted. However, due to technical limitations, this could not yet be realized in this work and would be the prospect for the next work.

Supplementary data to this article can be found online at https://doi.org/10.1016/j.scriptamat.2018.03.038.

Acknowledgement

This work was supported by the Research Council of Norway through the project HyF-Lex (project number: 244068/E30).

References

[1] H. Vehoff and P. Neumann, *Acta Metall.* **28** (3), 1980, 265–272.

[2] H. Vehoff and W. Rothe, *Acta Metall.* **31** (11), 1983, 1781–1793.

[3] M. Koyama, Y. Onishi and H. Noguchi, *Int. J. Fract.* **206** (1), 2017, 123–130.

[4] G. Bilotta, G. Henaff, D. Halm and M. Arzaghi, *Int. J. Hydrog. Energy* **42** (15), 2017, 10568–10578.

[5] Z. Sun, G. Benoit, C. Moriconi, F. Hamon, D. Halm, F. Hamon and G. Hénaff, *Int. J. Hydrog. Energy* **36** (14), 2011, 8641–8644.

[6] M. Dadfarnia, A. Nagao, S. Wang, M.L. Martin, B.P. Somerday and P. Sofronis, *Int. J. Fract.* **196** (1–2), 2015, 223–243.

[7] M. Dadfarnia, P. Sofronis, B.P. Somerday and I.M. Robertson, *Int. J. Mat. Res.* **99** (5), 2008, 557–570.

[8] J.A. Ronevich, B.P. Somerday and C.W. San Marchi, *Int. J. Fatigue* **82**, 2016, 497–504.

[9] B.P. Somerday, P. Sofronis, K.A. Nibur, C. San Marchi and R. Kirchheim, *Acta Mater.* **61** (16), 2013, 6153–6170.

[10] H. Matsunaga, M. Yoshikawa, R. Kondo, J. Yamabe and S. Matsuoka, *Int. J. Hydrog. Energy* **40** (16), 2015, 5739–5748.

[11] Y. Ogawa, D. Birenis, H. Matsunaga, A. Thøgersen, Ø. Prytz, O. Takakuwa and J. Yamabe, *Scr. Mater.* **140**, 2017, 13–17.

[12] J. Yamabe, M. Yoshikawa, H. Matsunaga and S. Matsuoka, *Int. J. Fatigue* **102**, 2017, 202–213.

[13] S. Wang, N. Hashimoto and S. Ohnuki, *Mater. Sci. Eng. A* **562**, 2013, 101–108.

[14] T. Depover, O. Monbaliu, E. Wallaert and K. Verbeken, *Int. J. Hydrog. Energy* **40** (47), 2015, 16977–16984.

[15] T. Depover, D. Pérez Escobar, E. Wallaert, Z. Zermout and K. Verbeken, *Int. J. Hydrog. Energy* **39** (9), 2014, 4647–4656.

[16] T. Depover and K. Verbeken, *Int. J. Hydrog. Energy* **41** (32), 2016, 14310–14329.

[17] T. Depover and K. Verbeken, *Mater. Sci. Eng. A* **669**, 2016, 134–149.

[18] T. Depover and K. Verbeken, *Mater. Sci. Eng. A* **675**, 2016, 299–313.

[19] T. Depover and K. Verbeken, *Corros. Sci.* **112**, 2016, 308–326.

[20] T. Depover, E. Wallaert and K. Verbeken, *Mater. Sci. Eng. A* **649**, 2016, 201–208.

[21] T. Depover, E. Wallaert and K. Verbeken, *Mater. Sci. Eng. A* **664**, 2016, 195–205.

[22] C. Lekbir, J. Creus, R. Sabot and X. Feaugas, *Mater. Sci. Eng. A* **578**, 2013, 24–34.

[23] Y. Deng, T. Hajilou, D. Wan, N. Kheradmand and A. Barnoush, *Scr. Mater.* **127**, 2017, 19–23.

[24] Y. Deng and A. Barnoush, *Acta Mater.* **142**, 2018, 236–247.

[25] B.R.S. Rogne, N. Kheradmand, Y. Deng and A. Barnoush, *Acta Mater.* **144**, 2018, 257–268.

[26] N. Narita, *Scr. Metall.* **18** (9), 1984, 985–988.

[27] A. Kimura and H.K. Birnbaum, *Scr. Metall.* **21** (1), 1987, 53–57.

[28] E. Malitckii, Y. Yagodzinskyy and H. Hänninen, *Fusion Eng. Des.* **98–99**, 2015, 2025–2029.

[29] A. Barnoush and H. Vehoff, *Acta Mater.* **58** (16), 2010, 5274–5285.

[30] A. Barnoush and H. Vehoff, *Corros. Sci.* **50** (1), 2008, 259–267.

[31] H. Vehoff, Rißbildung und Rißausbreitung in Ein- und Bikristallen, 1994, VDI-Verlag; Düsseldorf.

[32] H. Vehoff, Untersuchung der duktilen und quasispröden zyklischen Rißausbreitung in Fe-3%-Si-Einkristallen, PhD thesis, 1977, RWTH Aachen; Aachen.

[33] H. Vehoff, P. Neumann and W. Rothe, *Met. Sci.* **15** (10), 2013, 469–470.

[34] S.H. Chen, Y. Katz and W.W. Gerberich, *Philos. Mag. A* **63** (1), 1991, 131–155.

[35] Y. Mine, K. Koga, O. Kraft and K. Takashima, *Scr. Mater.* **113**, 2016, 176–179.

[36] A. Vesel, A. Drenik, R. Zaplotnik, M. Mozetic and M. Balat-Pichelin, *Surf. Interface Anal.* **42** (6–7), 2010, 1168–1171.

[37] G.M. Bond, I.M. Robertson and H.K. Birnbaum, *Scr. Metall.* **20** (5), 1986, 653–658.

[38] A. Kimura and H. Kimura, *Mater. Sci. Eng.* **77**, 1986, 75–83.

[39] H.K. Birnbaum, *Scr. Metall. Mater.* **31** (2), 1994, 149–153.

[40] D. Hull and D.J. Bacon, Introduction to Dislocations, fifth ed., 2011, Elsevier.

[41] T. Hajilou, Y. Deng, B.R. Rogne, N. Kheradmand and A. Barnoush, *Scr. Mater.* **132**, 2017, 17–21.

[42] J. Song and W.A. Curtin, *Nat. Mater.* **12** (2), 2013, 145–151.

The following is the supplementary data related to this article.

Multimedia Component 1 

Supplementary video

alt-text: Image 1

Graphical abstract

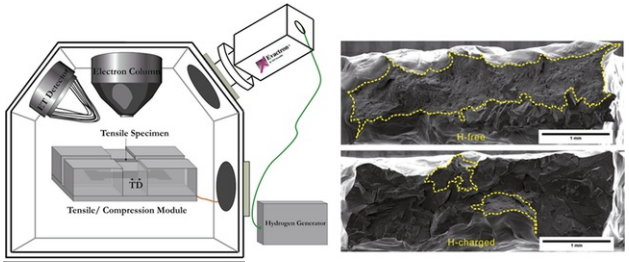

alt-text: Unlabelled Image

Queries and Answers

Query:

Your article is registered as a regular item and is being processed for inclusion in a regular issue of the journal. If this is NOT correct and your article belongs to a Special Issue/Collection please contact a.rassette@elsevier.com immediately prior to returning your corrections.

Answer: Yes

Query:

Please confirm that given names and surnames have been identified correctly and are presented in the desired order, and please carefully verify the spelling of all authors' names.

Answer: Yes

Query:

The author names have been tagged as given names and surnames (surnames are highlighted in teal color). Please confirm if they have been identified correctly.

Answer: Yes